



Mechanism of TCO thin film removal process using near-infrared ns pulse laser: Plasma shielding effect on irradiation direction



Byunggi Kim^{a,*}, Ryoichi Iida^a, Hong Duc Doan^{a,b,*}, Kazuyoshi Fushinobu^a

^a Department of Mechanical and Control Engineering, Tokyo Institute of Technology, Mail Box 16-3, Ookayama 2-12-1, Meguro-ku, 152-8552, Japan

^b Advances Materials and Structures Laboratory, University of Engineering and Technology, Vietnam National University, Hanoi, 144 Xuan Thuy, Cau Giay, Hanoi, Viet Nam

ARTICLE INFO

Article history:

Received 10 March 2016

Received in revised form 1 June 2016

Accepted 5 June 2016

Keywords:

Nanosecond laser scribing

Laser ablation

Transparent conductive oxide thin film

Plasma shielding

ABSTRACT

Substrate side irradiation is widely used for a thin film removal process because high absorption at the film/substrate or film/film interface leads to complete isolation of thin film by single shot irradiation of laser pulse with low energy. However, in the transparent thin film removal process, large thermal expansion or local phase change at the interface cannot be created by substrate side irradiation because of its large optical penetration depth compared to its small thickness. Nevertheless, substrate side irradiation works obviously for single shot film isolation process compared to film side irradiation, and the mechanism of the process was not clear in terms of difference in the irradiation direction. In order to investigate the effect of the irradiation direction, this study focused on the transient interaction between the material and nanosecond laser pulse. Experimental results showed that film was thermally ablated. Variation of temporal profile of nanosecond laser pulse during the process was experimentally investigated to detect plasma shielding. Pulse width and energy transmittance of transmitted pulse decreased by plasma shielding as pulse energy increases regardless of irradiation direction. In addition, temperature distribution in the film during the process was investigated using a 2-dimensional thermal model, which accounts for melting, vaporization, and laser induced plasma shielding. Calculated temperature distribution was used to support the scenario of the process mechanism which was investigated in the experiments. Our findings demonstrate that laser induced backward ablation is a single shot TCO film removal mechanism, and plasma shielding is dominant factor to interrupt absorption of beam thorough the film in the film side irradiation process.

© 2016 Elsevier Ltd. All rights reserved.

1. Introduction

Use of transparent conductive oxide (TCO) thin film is widely increasing with a spread of various opto-electronical technologies such as touchscreens, liquid crystal display, and photovoltaics. Indium tin oxide (ITO), fluorine doped tin oxide (FTO), and zinc oxide (ZnO) films are most widely used materials as a TCO thin film. Electrical conductivity of these TCO thin films must be ensured while they have very thin thickness of nanometers order for the sufficient transmission as an optical window. Due to the TCOs' high transparency on the wide range of visible and infrared spectra, the optical penetration depth is usually longer than the thickness of the thin films. Therefore, thin film removal processing using laser single shot ablation can be effectively used for patterning of the TCO thin films. In addition, as a nanosecond laser

scribing with 1064 nm/532 nm wavelength can be implemented industrially with m/s order processing speed [1–5], it is significantly advantageous for the fabrication of scribes on the thin film photovoltaic (TFPV) devices, which necessarily need use of large size transparent thin film layers of meter square order deposited on transparent substrate.

Making the scribes on the thin film layers of the TFPV devices allow implementation of efficient low-current/high-voltage devices. On the other hand, the width of the grooves must be minimized because area of the scribes is counted as a dead area that cannot generate electricity with solar irradiation. Of course, formation of heat-affected zone (HAZ) by ns laser irradiation must be taken into account as well. Hence, there is no doubt that understanding the thin film removal mechanism is critically important for optimum implementation of fabrication system as to curtail the heat affected zone with narrow groove width.

Fig. 1 represents schematic illustration of basic mechanisms of the laser substrate side scribing process. For the thin film with high absorbance, absorption of laser beam takes place at the vicinity of

* Corresponding authors. Tel.: +81 3 5734 2500 (B. Kim).

E-mail addresses: kim.b.aa@m.titech.ac.jp (B. Kim), doan.d.aa.eng@gmail.com (H.D. Doan).

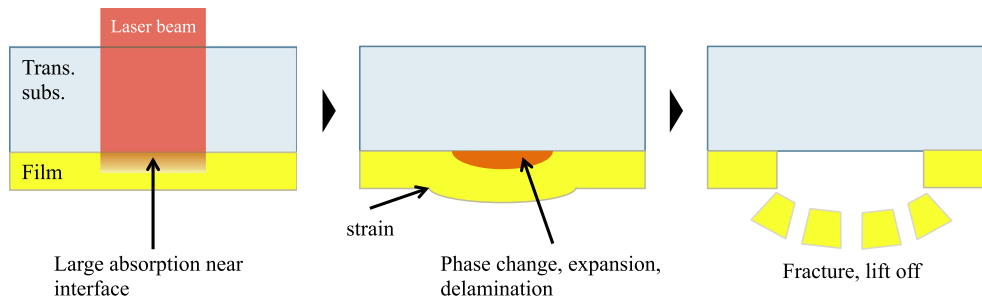


Fig. 1. Schematic illustration of basic mechanism of thin film removal processing by substrate side irradiation. For the thin film with high absorption coefficient, most illuminated laser beam is absorbed at the vicinity of the interface. Local thermal ablations such as vaporization and formation of plasma lead to stress assisted removal of thin film by a single shot.

interface between thin films or thin film/substrate. In this case, relatively low fluence of laser beam can cause the thermal expansion, local vaporization, or generation of plasma at the interface so that stress-assisted ablation is dominant to remove thin film. Several studies have demonstrated theoretical models to explain the thin film removal mechanism. Several researchers used pure thermal model to discuss mechanism by means of temperature profile and phase change [6–8]. Also, formation of micro/nanobump has been under consideration of several studies [9,10]. The approximate thermoelastic solution of round plate with fixed edge to describe initial thermal stress given on laser heated thin films [1,9,10]. Also, plasma induced pressure for lift off or peening of target materials was experimentally and theoretically studied in several works [11,12]. It is shown obvious that confined geometry with transparent substrate or liquid results in formation of significantly high pressure during adiabatic cooling of plasma [11–17].

However, feature of the TCO thin film removal processing is more complicated because it has relatively larger optical penetration depth than its thickness as mentioned above. Temperature profile along optical axis is not certainly different whether laser beam is irradiated from film side or substrate side, which means that stress-assisted ablation is rather difficult to happen. In several researchers' works [3,18], film side irradiation needed higher fluence for complete isolation of the film by single shot. In addition, profiles of the craters formed by single shot irradiation were significantly different according to the irradiation direction. Wang et al. [4] used thermoelastic models to explain the TCO thin film removal mechanism. Their findings show that the film can be removed without phase change although temperature profile along the optical axis is almost uniform, if principle stress exceeds materials strengths. However, there are still experimentally unclear things

remained concerned with difference between film side and substrate side irradiation.

In this study, therefore, we aimed to investigate the mechanism of the TCO thin film removal process focusing on the direction of the irradiation. Using ns laser pulse of 1064 nm, parametric studies on the FTO thin film removal process are given first. Previous studies [19–23] have shown that inverse Bremsstrahlung reflection and absorption prevent incoming laser pulse to reach materials surface, so that mass ablation rate and temporal profile of reflected and transmitted pulses changes transiently. Under consideration of this knowledge, we measured transmitted pulse profile to examine those effects. As analyzing the experimental results, thermal model is used to predict the TCO thin film removal mechanism in the later section.

2. Experimental methods

Fig. 2 shows schematic illustration of experimental setup. Nanosecond laser irradiation system was prepared to process the FTO thin film on soda lime glass sample (Asahi type-VU). This sample has texturized surface with roughness of 20–30 nm for improvement of light trapping as it has been designed for the use in the TFPV devices [24]. Nd:YAG fundamental wave (1064 nm), of which pulse width is 5–7 ns, was used in this study. This fundamental wavelength indicates relatively large absorption into the FTO film with high oscillation efficiency. Original beam was expanded and transmitted through circular aperture to obtain circular top-hat profile. The top-hat beam was focused by plano-convex lens ($f = 100$ mm) to be shaped into a narrow Gaussian beam with radius of 12 μm . Once threshold fluence of film damage

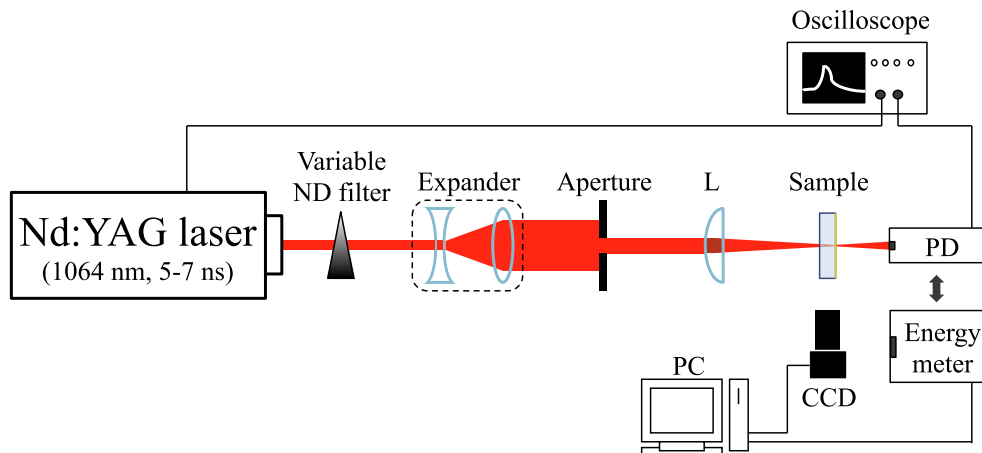


Fig. 2. Schematic illustration of experimental apparatus. Photodiode and energy meter were prepared to detect effects of plasma shielding.

Table 1
Experimental parameters.

Parameter	Unit	Value
Wavelength, λ	nm	1064
Pulse width, t_p	ns	5–7
Focal length, f	mm	100
Beam radius at focus, w_0	μm	12
FTO thickness, h	nm	600–700
Substrate thickness	mm	1.8

was found, the fluence was increased to investigate the effect of the beam fluence on the crater profiles. Except for threshold fluence, all the fluences described in this paper are peak fluence of a Gaussian beam.

Photodiode, of which rise time is <2 ns, and energy meter were alternately used for the measurement of change of pulse temporal profile and energy transmissivity of pulse through the sample during process respectively. These measurements allow the performance of observation of plasma shielding. If plasma shielding by

ablated materials is significant, backward of the pulse would be curtailed so that we can affirm change of temporal profile and noticeable energy decrease of transmitted pulse [20,21,23]. All the experiments were performed in room condition. Experimental parameters are tabulated in Table 1.

3. Results and discussion

3.1. Film removal threshold and quality

Fig. 3 shows confocal microscope images of fabricated film and cross-sectional profile of the craters with different intensities. Craters with smooth taper were fabricated. Canteli et al. [3] said that the fabrication results of the FTO thin film with IR light shows craters with smooth taper due to melted and re-solidified material. Same interpretation may be valid in the present context, as craters have similar boundary which has melted and re-solidified structure and smooth taper rather than crack formation. Note that craters without complete film removal indicate uneven surface

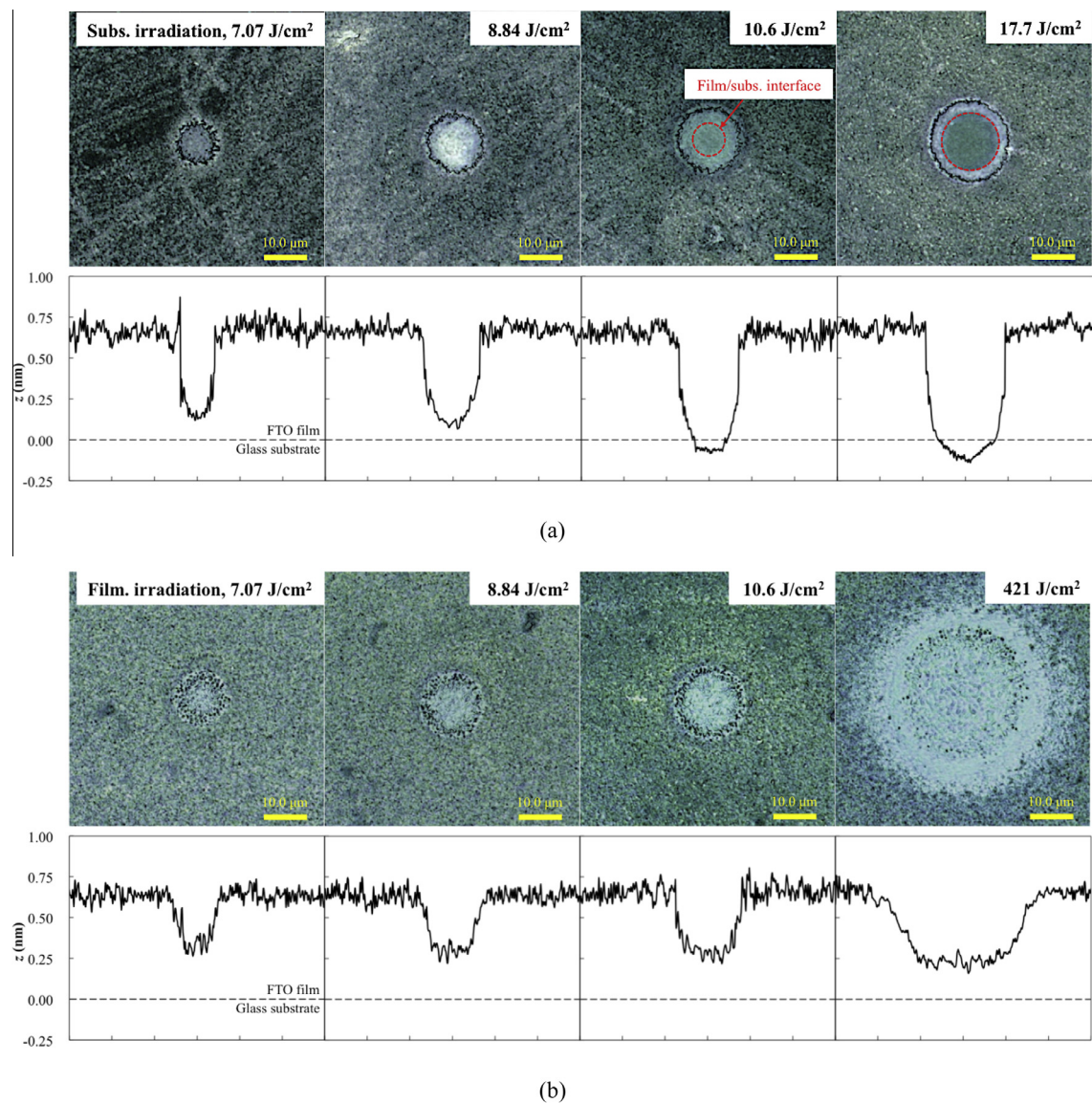


Fig. 3. Confocal microscope images and cross-sectional profiles of fabricated craters. Upper row (a) and under row (b) show the results by substrate side and film side irradiations respectively. Thin film was ablated from the surface regardless of irradiation direction. Substrate side irradiation needed only 10.6 J/cm² to achieve complete film removal, while film side irradiation could not achieve complete film removal with 421 J/cm².

profile. It is considered that texturized film surface may affect absorption profile along the optical axis direction. Furthermore, re-solidification of the film material may result in formation of the pattern on the surface.

Another interesting thing is that film ablation occurs from the surface regardless of the irradiation direction. The followings may explain this behavior well.

- In the nanosecond regime, heat flow from the film surface to ambient air is ignorable compared to heat conduction from the film to the substrate.
- Light absorption is almost homogeneous along the optical axis through the film. Compared to the film surface, more heat is conducted from bottom of the film to the glass substrate due to relatively high heat conductivity. As a result, temperature rise is much higher near the surface of the film.
- This leads to the first ablation at the surface.

Therefore, the film may be ablated from the surface, and ablation thickness increases with larger fluence to remove the whole film thickness. This process is to be described later in details in Section 3.3.

Film damage threshold was 4.8 J/cm^2 regardless of the irradiation direction. The complete film removal was achieved with the fluence of 10.6 J/cm^2 with the substrate side irradiation. Steep change of cross sectional profile is shown at the film/substrate interface in this regime. However, it was not achieved even with the significantly large fluence of 421 J/cm^2 in the case of film side irradiation. Although film damage thresholds were almost same, the complete removal of the film was strongly dependent on the irradiation direction. This implies that certain factor disturbs development of ablation depth with the film side irradiation.

Fig. 4 shows width and depth of the craters as a function of the fluence. The crater width increased with increase of the fluence regardless of the irradiation direction. Width of the beam defined by the threshold fluence is represented in the Fig. 4(a), too. The crater width well agreed with this width. It is natural that size of ablated area well matches with the size of the irradiated area over the threshold in the nanosecond thermal ablation process. In the case of substrate side irradiation, depth of the crater became gradually larger to reach the glass substrate even over the film thickness. Temperature rise of the glass substrate over softening point (see Section 3.2 and Table 2) due to heat conduction from the film accounts for this ablation at a high fluence. Therefore, pulse energy must be well optimized to avoid critical substrate damage. On the other hand, in the case of film side irradiation, the crater depth was hardly enlarged with increase of the fluence. These behaviors characterized by the irradiation direction will be discussed in the next section in terms of the plasma shielding effect.

3.2. Influence of plasma shielding

Fig. 5 indicates the change of pulse temporal profile and pulse duration of the first pulse after processing. In Fig. 5(a) and (b), the original pulse temporal profile is also indicated for the comparison, and all the profiles are normalized for its own peak intensity. In Fig. 5(a) and (b), temporal profile of the pulse after processing has steep declining compared with original pulse so as to result in decrease of the pulse width (Fig. 5(c)). These results show exactly the same effect demonstrated by Wolff-Rottke et al. [20,21] and Mao et al. [23]. Their studies showed that backward of temporal pulse is curtailed by plasma shielding. It would be reasonable to consider that the plasma rises with significantly larger fluence than threshold during the process of thermal ablation. Of course, the more intensive laser beam is illuminated, the faster plasma rises so that pulse duration gets far shorter. In effect, we

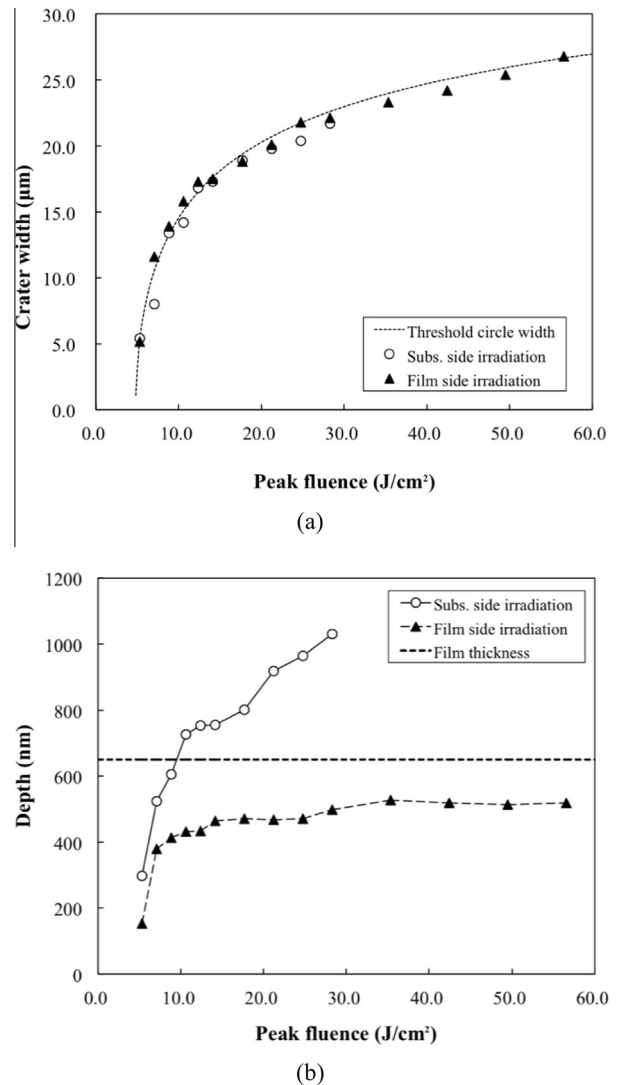


Fig. 4. Parameters of the fabricated craters. (a) Width of the craters. (b) Depth of the craters. The width of the craters well agreed with that of threshold circles. Ablation depth of the substrate side irradiation increased with the fluence to reach and damage the glass substrate.

could observe the plasma plume as a burst of white light by the naked eyes during the process with fluence larger than or equal to 8.84 J/cm^2 .

As plasma is generated at the surface of the film, this transient plasma shielding during pulse duration interrupts sufficient absorption of the whole pulse for the complete film removal in the case of film side irradiation. However, in the case of substrate side irradiation, whole pulse can be absorbed temporally as pulse reaches film before reaching to plasma. Thus, we can conclude that laser induced backward ablation leads to complete removal of the TCO film, and plasma shielding at the surface make directional effect in this process. In addition, not only for thin film laser scribing, but also for bulk material laser ablation, plasma shielding must be considered to optimize processing parameters to prevent waste of laser pulse energy.

Fig. 6 shows variation of transmissivity of the laser pulse through the sample by means of number of illuminated pulses. Several initial pulses, which induce ablation of the FTO film, have low energy transmissivity. Here, obvious difference can be seen with respect to the irradiation direction. In the case of substrate side irradiation, the transmissivity increased to reach 'steady state' (here we define it as a constant transmissivity after illumination of

Table 2
Physical properties of materials.

Parameter	Unit	SnO ₂ [29,30] (temperature (K))	Glass
Density	kg/m ³	6950	2520
Specific heat, c_p	J/kg K	$3520 \times 10^{-4} \cdot T + 200$ $7750 \times 10^{-5} \cdot T + 475$ 614	837
Latent heat of melting, L_m	J/kg	3.17×10^5	–
Melting temperature, T_m	K	1898	722 (softening)
Latent heat of vaporization, L_v	J/kg	2.08×10^6	–
Boiling temperature, T_v	K	2273	–
Thermal conductivity, k	W/m K	30 $4540/T^{0.88}$ 5	1
Absorption coefficient, α^*	m ⁻¹	1.5×10^5	–
A^{***}	m ⁻¹	1.5×10^6	–
B^{***}	m ² /J	9.6×10^{-4}	–
Half range of phase change, Δ	K	50	–
Film thickness, h^{**}	nm	650	–
Refractive index, n	–	1.6 [4] at 1064 nm	1.51 at 1064 nm

* Based on measurement in this study.

** Based on sample specification.

*** Based on experimental results in this study.

5 pulses in each cases) within 2–3 pulses because of complete removal of the film in early stage. However, film side irradiation required at least 4 pulses to reach steady state as remained film was fabricated by second or third pulse.

When film was not removed completely by first irradiation, transmissivity of the second pulse indicated even lower value than that of first pulse (i.e. 8.84, 28.3 J/cm² of film side irradiation). Change of optical properties of the film caused by first pulse ablation may account for this behavior. We can predict that re-solidified FTO has stronger optical absorption.

3.3. Thermal modeling and analysis

In the previous sections, we experimentally demonstrated that the TCO thin film is removed from its surface by thermal ablation, and absorption of the beam is disturbed by plasma shielding with the film side irradiation. This scenario would be more persuasive if craters' profiles (Fig. 3) have critical relationship with temperature distributions during process. Thus, we solved simple 2D unsteady heat conduction equation to investigate temperature distributions during the process. Cylindrical coordinates were set because a Gaussian laser beam has an axial symmetry. Region of interest for numerical calculation is shown in Fig. 7. For pulsed laser ablation, melting, vaporization and, effect of plume shielding on source term can be implemented in the heat equation [25–28]. The temperature distribution in a cylindrical coordinates system is governed by the following equation:

$$\rho [c_p + L_m \delta(T - T_m)] \left(\frac{\partial T}{\partial t} - v_s \frac{\partial T}{\partial z} \right) = k \left(\frac{1}{r} \frac{\partial T}{\partial r} + \frac{\partial^2 T}{\partial r^2} + \frac{\partial^2 T}{\partial z^2} \right) + S \quad (1)$$

where c_p , ρ , L_m , T_m , v_s , k , and S indicate specific heat, density, latent heat of melting, melting temperature, surface recession velocity, thermal conductivity, and source term respectively. Surface recession velocity is defined under the assumption that the flow of vaporized material from the surface follows the Hertz–Knudsen equation and the vapor pressure above the vaporized surface can be estimated with the Clausius–Clapeyron equation [27,28].

$$v_s = (1 - \beta) \left(\frac{M}{2\pi k_B T_s} \right)^{1/2} \frac{p_0}{\rho} \exp \left[\frac{ML_v}{k_B} \left(\frac{1}{T_v} - \frac{1}{T_s} \right) \right] \quad (2)$$

Here, M , k_B , T_s , p_0 , L_v , and T_v indicate atomic mass, Boltzmann constant, surface temperature, reference pressure, latent heat of vaporization, and boiling temperature respectively. β is so called sticking coefficient which accounts for the back-flux of the ablated species, being approximately 0.18 [27,28]. Source term S expresses laser beam absorption with a Gaussian spatial and temporal profile in the FTO film with following forms.

$$S_s = \alpha (1 - R_{\text{Glass}/\text{Air}}) (1 - R_{\text{Glass}/\text{TCO}}) \frac{2E_p}{\pi w_0^2} \exp \left(-\frac{2r^2}{w_0^2} \right) \cdot \frac{2\sqrt{\ln 2}}{t_p \sqrt{\pi}} \exp \left[-4 \ln 2 \cdot \left(\frac{t - 2t_p}{t_p} \right)^2 \right] \cdot \exp[\alpha(z - h)] \quad (3.1)$$

$$S_f = \alpha (1 - R_{\text{TCO}/\text{Air}}) \frac{2E_p}{\pi w_0^2} \exp \left(-\frac{2r^2}{w_0^2} \right) \cdot \frac{2\sqrt{\ln 2}}{t_p \sqrt{\pi}} \exp \left[-4 \ln 2 \cdot \left(\frac{t - 2t_p}{t_p} \right)^2 \right] \cdot \exp[-\alpha z] \cdot \exp(-A \cdot dZ - B \cdot E_a) \quad (3.2)$$

Here, Eqs. (3.1) and (3.2) are for substrate side irradiation and film side irradiation respectively. α , R , E_p , L , h , dZ , and E_a indicate absorption coefficient, reflectance, pulse energy, thickness of glass of numerical interest, film thickness, vaporized depth, and laser fluence absorbed by plasma plume respectively. Subscripts of R indicate the interface where each R is applied. Temporal peak of the pulse was set at $2t_p$. By using the term $\exp(-A \cdot dZ - B \cdot E_a)$ at the end of Eq. (3.2), fluence attenuation due to plasma shielding is calculated in the case of film side irradiation. Here, this term was not used in the case of substrate side irradiation because the laser pulse does not experience plasma shielding before absorption. A and B are plasma absorption coefficients which determine the contribution of amount of vaporized material and absorbed energy to plasma density respectively. A and B are free parameters which can be determined based on experimental results. In specific cases when the plasma absorption mechanism is well established, A and B can be estimated theoretically [26].

In Eq. (1), the term $L_m \delta(T - T_m)$ with the Kronecker δ -like function of the form:

$$\delta(T - T_m, \Delta) = \frac{1}{\sqrt{2\pi}\Delta} \exp \left[-\frac{(T - T_m)^2}{2\Delta^2} \right] \quad (4)$$

allows the performance of calculation of the liquid–solid interface [25,26,28]. Half range of phase change Δ is to be set in the range

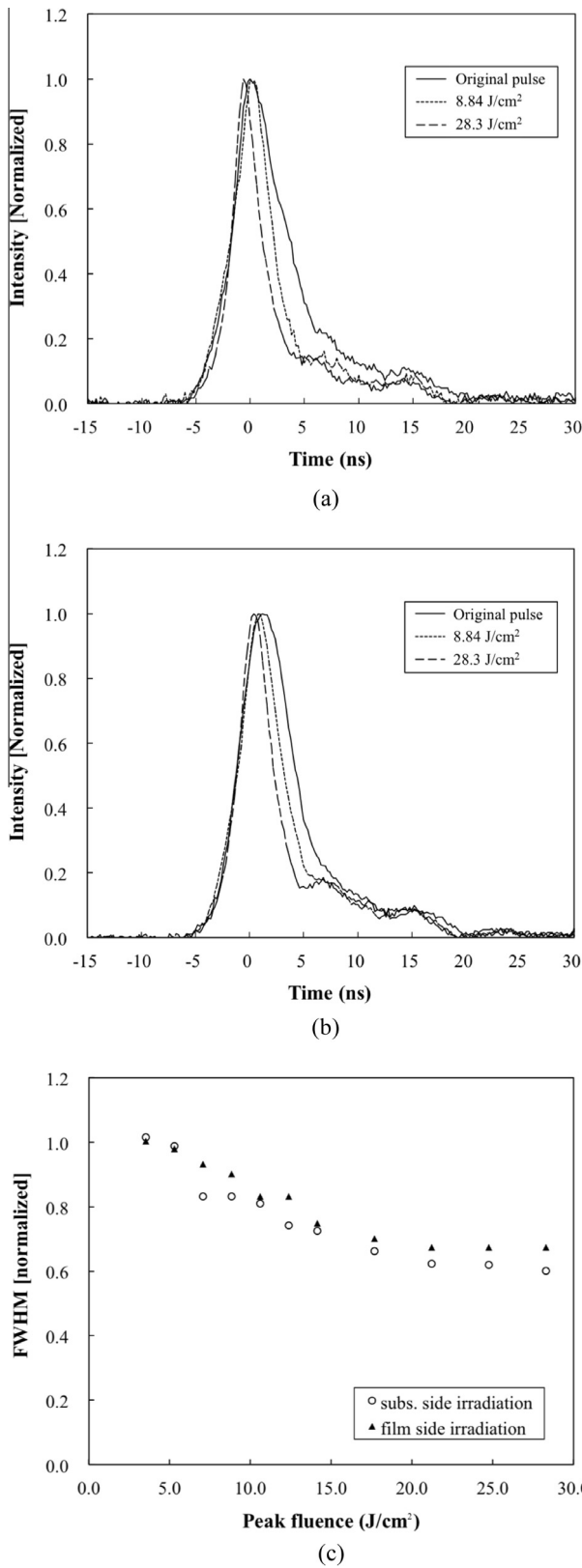


Fig. 5. Variation of the laser pulse temporal profile after processing. Normalized pulse temporal profiles compared with the original profile with (a) substrate side irradiation and (b) film side irradiation. In (a) and (b), solid line indicates original pulse temporal profile. Dotted line and dashed line indicate pulse temporal profile of 8.84 J/cm² and 28.3 J/cm² respectively. In both cases, declining part of the pulses was steepened by inverse Bremsstrahlung. (c) Pulse duration change after processing. Circle and colored triangle indicate results of substrate side irradiation and film side irradiation respectively. As plasma rises quickly with large fluence, pulse duration gradually became shorter with increase of fluence.

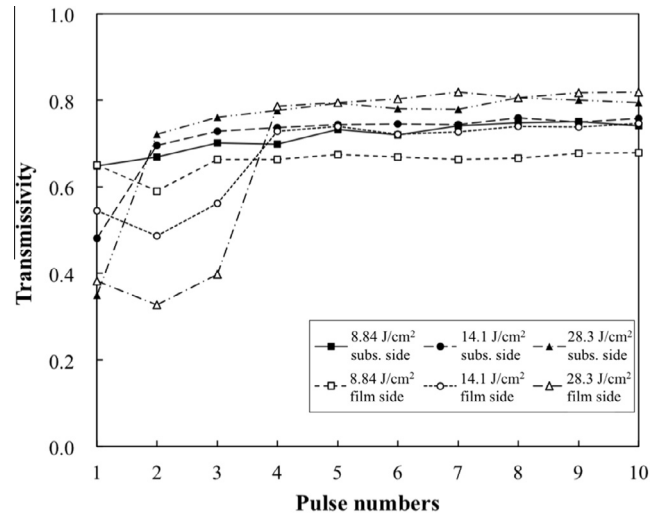


Fig. 6. Variation of transmissivity of the laser pulse through the sample by means of number of illuminated pulses. Solid rectangular, solid circle, solid triangle indicate the substrate side irradiation cases of 8.84 J/cm², 14.1 J/cm², and 28.3 J/cm², respectively. Hollow rectangular, solid circle, solid triangle indicate the film side irradiation cases of 8.84 J/cm², 14.1 J/cm², and 28.3 J/cm² respectively. Film side irradiation requires more pulse numbers to steady state than substrate side irradiation because film is not completely removed by the first pulse illumination.

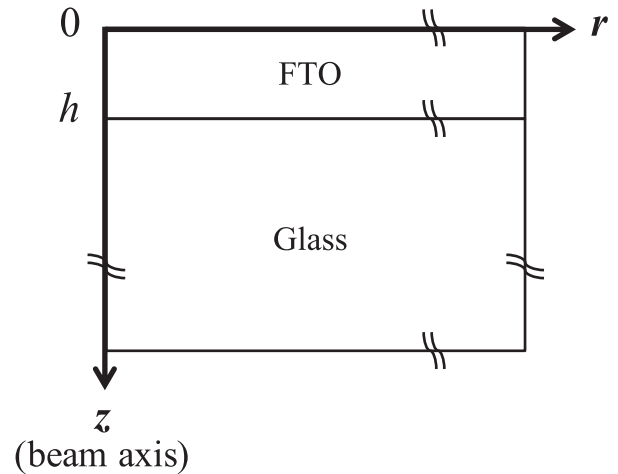


Fig. 7. Schematic illustration of modeling region. Axial symmetry of a laser beam provides the implementation of cylindrical coordinates system.

of 10–100 K depending on temperature gradient. At least three computational cells must be included in the range [25]. In the present context, we set Δz as 50 K.

In the nanosecond regime, heat flux of natural convection and radiation heat transfer is in order of 10⁴–10⁵ W/m² which is ignorable compared to heat flux of conduction to the substrate, of which order is 10⁸–10⁹ W/m². Hence, only the energy flux, which determines the surface vaporization of the sample during the laser pulse, was taken into account at the surface [28]. Also, no heat flow exists crossover z axis in cylindrical coordinates system as it has axial symmetry. The interface of glass/FTO can be considered as coupled boundary. Temperature boundary condition of $T = 300$ K, which is the value set as initial temperature, was defined at far boundaries in the direction of r and z. Above boundary conditions are applied as following forms.

$$\frac{\partial T}{\partial z}\Big|_{z=0} = \rho v_s L_v, \quad \frac{\partial T}{\partial r}\Big|_{r=0} = 0, \quad k_{\text{FTO}} \frac{\partial T}{\partial z}\Big|_{z=h} = k_{\text{Glass}} \frac{\partial T}{\partial z}\Big|_{z=h},$$

$$T(W, z) = T(r, 0) = 300 \text{ K} \tag{5}$$

In this study, implicit numerical scheme of finite differential method was implemented. Physical properties of materials are tabulated in Table 2. Temperature dependence of several thermal properties was considered [29,30]. Absorption coefficient α was obtained by inverse operation based on the measurement of transmissivity of the sample using following relationship between absorbance A , transmissivity τ , and reflectance R .

$$A = 1 - (R + \tau) \tag{6}$$

Fig. 8 shows calculation result of transient change of axial temperature at the fluence of 10.6 J/cm². Regardless of irradiation direction, temperature increases considerably at the vicinity of the film surface rather than at the vicinity of the film/substrate interface, because of the heat conduction through the interface. Therefore, we can confirm the scenario that thermal ablation begins from the film surface, then develops to the film/substrate interface. The case of substrate side irradiation indicates the largest temperature increase inside the film due to absorption profile along the film. Melting process may initiate inside film not from its surface. However, before inner melted area is ablated, surface temperature may reach melting temperature. Thus, thermal ablation of film is performed from the surface. It explains two experimentally seen characteristics in Figs. 3 and 4(b). In Fig. 3, craters fabricated by substrate side irradiation have steeper side slope in the direction of z axis compared to those fabricated by film side irradiation. Furthermore, in Fig. 4(b), craters fabricated by substrate side irradiation have larger depth at low fluence regime, where plasma shielding is not yet significant. The larger temperature increase inside the film may have a significant impact on these effects.

In experimental results (Fig. 3), craters keep texturized surface at their boundary so that we can expect that most of melted part of the film has been removed by melt-ejection or evaporation. Therefore, we will discuss about crater size in terms of melted area. Fig. 9 shows calculated 2-dimensional temperature distributions in the case of film side irradiation at 16.5 ns, when most of the pulse

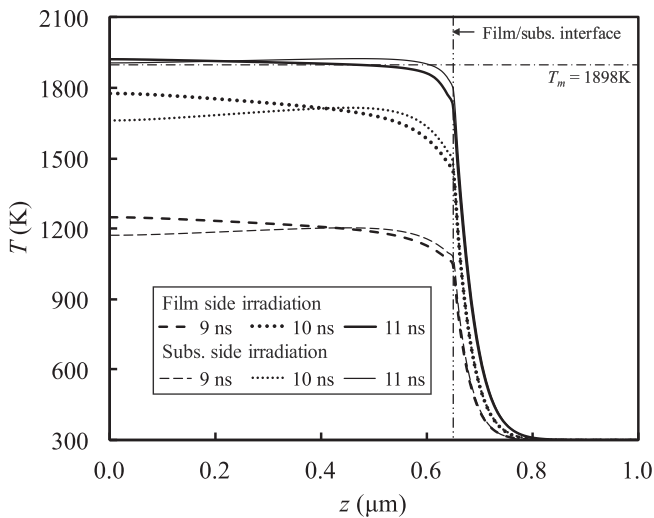


Fig. 8. Calculation results of transient change of axial temperature at 10.6 J/cm². Bold lines and narrow lines indicate the case of film side irradiation and substrate side irradiation respectively. Dashed, dotted, and solid lines indicate the results at 9 ns, 10 ns, 11 ns respectively. Temperature at the vicinity of the interface does not increase significantly due to conduction to the substrate.

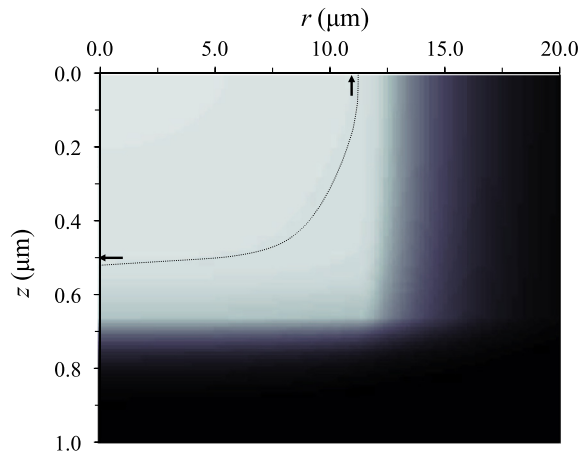
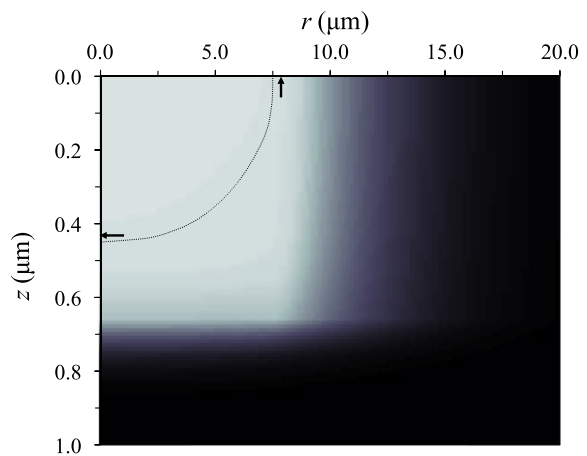
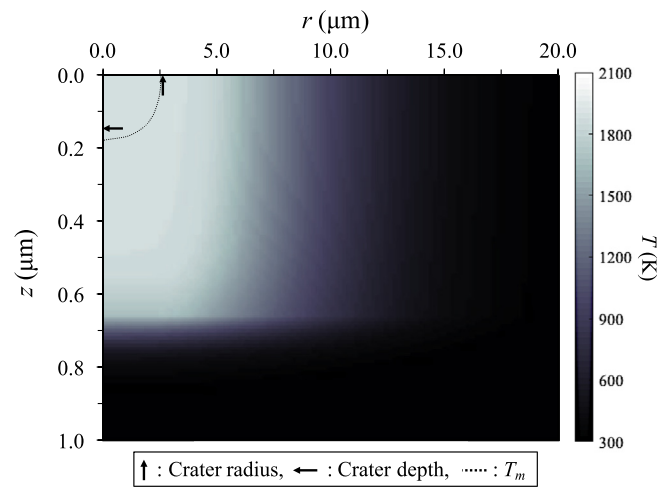


Fig. 9. Calculation results of 2-dimensional temperature distribution at 16.5 ns in the case of film side irradiation. (a) 5.3 J/cm², (b) 10.6 J/cm², (c) 28.3 J/cm². Dotted contour lines indicate melting temperature. Arrows indicate experimentally obtained radius and depth of craters. Color bar next to (a) is applied for (a)–(c). Most of melting area may be ablated during the process.

energy is absorbed. Melting depth and width well agrees with the craters' depth and width over the wide range of fluence. Similarly to experimental results shown in Fig. 4(b), melting depth does not increase significantly from 10.6 J/cm² to 28.3 J/cm². For entire range of fluence, crater depth was slightly smaller than melting depth. Expansion of substrate due to glass transition and re-solidification of the film may be responsible for the difference,

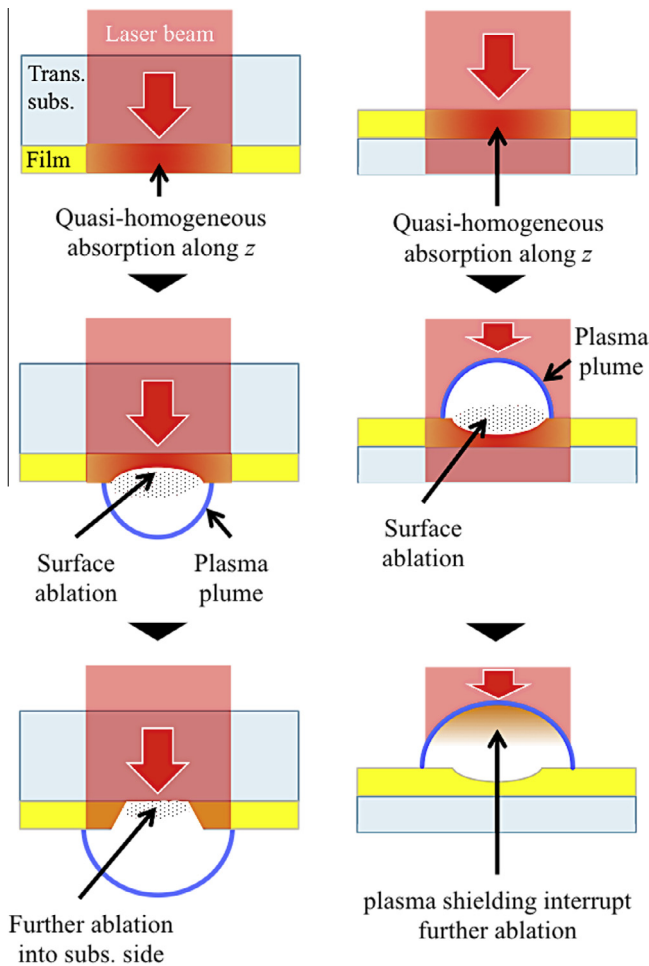


Fig. 10. Mechanism of the TCO thin film removal in laser scribing process. Plasma shielding disturbs development of thermal ablation toward substrate in the case of film side irradiation.

but not prominent. The TCO film ablation process was well expressed using the model which accounts for pulsed laser induced plasma shielding without considering stress-assisted ablation.

Regardless of irradiation direction, temperature of the glass near the interface is expected to increase far over its softening point at the early stage in the low fluence regime. Therefore, it is obvious that the substrate is significantly damage sensitive in the TCO film removal process investigated in this study. We would like to emphasize again that laser fluence must be adjusted delicately to avoid critical substrate damage.

3.4. Single shot film removal mechanism

We have experimentally and theoretically shown that plasma shielding has significant effect on film ablation in the case of film side irradiation, because the film ablation occurs from its surface. Fig. 10 illustrates this process by means of comparison on irradiation direction. The mechanism of nanosecond laser scribing for the TCO film removal by single shot can be summarized as below.

- Quasi-homogeneous absorption along z -direction leads to surface ablation with plasma.
- Ablation depth develops by continuous absorption irrespective of plasma shielding in the case of substrate side irradiation. On the other hand, plasma shielding disturbs development of ablation depth by inverse Bremsstrahlung reflection and absorption in the case of film side irradiation.

(c) Therefore, single shot film removal can be easily achieved with substrate side irradiation.

4. Conclusion

Experimental and theoretical investigations have been performed to understand the mechanism of nanosecond laser scribing of the TCO film on transparent substrate. The focus of this study was on the different processing results due to irradiation direction. The findings demonstrate the film ablation occurs from its surface regardless of irradiation direction, and laser induced backward ablation leads to complete removal of the film by single shot in the case of substrate side irradiation. However, it is difficult to achieve single shot film removal by film side irradiation because plasma shielding on the film surface disturbs sufficient absorption of the laser pulse during the process. This mechanism explains that plasma shielding must be considered as critical factor to avoid waste of pulse energy, not only for the process described in this study, but also for other nanosecond laser process using thermal ablation. In addition, we showed that pulse energy must be set carefully for design of nanosecond laser system for thin film scribing in order to minimize substrate damage.

Nevertheless, we would like to consequently note that film side irradiation can still be used for single shot film removal process, as our experimental results showed that it removed film thickness up to 500 nm by a pulse. For substrate materials with more significant light absorption or physical/chemical transmutability, it may be more suitable method to avoid unexpected damage through substrate that can occur in substrate side irradiation.

Acknowledgments

Part of this work has been supported by JSPS KAKENHI Grant Number 15J10556 and Amada Foundation. B. Kim represents special gratitude to JSPS.

References

- J. Bovatsek, A. Tamhankar, R.S. Patel, N.M. Bulgakova, J. Bonse, *Thin Solid Films* 518 (2010) 2897–2904.
- D. Canteli, S. Fernandez, C. Molpeceres, I. Torres, J.J. Gandía, *Appl. Surf. Sci.* 258 (2012) 9447–9451.
- D. Canteli, I. Torres, J.J. García-Ballesteros, J. Càrabe, C. Molpeceres, J.J. Gandía, *Appl. Surf. Sci.* 271 (2013) 223–227.
- H. Wang, S.T. Hsu, H. Tan, Y.L. Yao, H. Chen, M.N. Azer, *J. Manuf. Sci. Eng.* 135 (2013) 051004.
- S.F. Tseng, W.T. Hsiao, D. Chiang, C.K. Chung, J.L.A. Yeh, *Opt. Lasers Eng.* 52 (2014) 212–217.
- S. Kiyama, Y. Hirono, H. Hosokawa, T. Moriguchi, S. Nakano, M. Osumi, *JSPE* 56 (1990) 1500–1506 (in Japanese).
- N. Angelucci, N. Bianco, O. Manca, *Int. J. Heat Mass Transfer* 40 (1997) 4487–4491.
- S. Avagliano, N. Bianco, O. Manca, V. Naso, *Int. J. Heat Mass Transfer* 42 (1999) 645–656.
- Y.P. Meshcheryakov, N.M. Bulgakova, *Appl. Phys. A* 82 (2006) 363–368.
- Y.P. Meshcheryakov, M.V. Shugaev, T. Mattie, T. Lippert, N.M. Bulgakova, *Appl. Phys. A* 113 (2013) 521–529.
- R. Fabbro, J. Fournier, P. Ballard, D. Devaux, J. Virmont, *J. Appl. Phys.* 68 (1990) 775–784.
- W. Zhang, Y.L. Yao, I.C. Noyan, *J. Manuf. Sci. Eng.* 126 (2004) 10–17.
- P. Zhang, Y. Qin, J. Zhao, B. Wen, Y. Cao, Z. Gong, *J. Phys. D: Appl. Phys.* 42 (2009) 225302.
- P. Peyre, R. Fabbro, *Opt. Quantum. Electron.* 27 (1995) 1213–1229.
- S. Zhu, Y.F. Lu, M.H. Hong, *Appl. Phys. Lett.* 79 (2001) 1396–1398.
- S. Zhu, Y.F. Lu, M.H. Hong, X.Y. Chen, *J. Appl. Phys.* 89 (2001) 2400–2403.
- R. Karimzadeh, J.Z. Anvari, N. Mansour, *Appl. Phys. A* 94 (2009) 949–955.
- V.V. Matyilitsky, H. Huber, D. Kopf, *Proc. ICALEO 2011* (2011) M903.
- V. Tokarev, W. Marine, J.G. Lunney, M. Sentis, *Thin Solid Films* 241 (1994) 129–133.
- B. Wolff-Rottke, J. Ihlemann, H. Schmidt, A. Scholl, *Appl. Phys. A* 60 (1995) 13–17.
- J. Ihlemann, A. Scholl, H. Schmidt, B. Wolff-Rottke, *Appl. Phys. A* 60 (1995) 411–417.
- R.K. Singh, *J. Electron. Mater.* 25 (1996) 125–129.

- [23] X. Mao, R.E. Russo, *Appl. Phys. A* 64 (1997) 1–6.
- [24] M. Kambe, N. Taneda, A. Takahashi, T. Oyama, *Res. Reports Asahi Glass Co., Ltd.* 60 (2010) (in Japanese).
- [25] S.P. Zhvavyi, G.D. Ivlev, *J. Eng. Phys. Thermophys.* 69 (1996) 608–611.
- [26] N.M. Bulgakova, A.V. Bulgakov, L.P. Babich, *Appl. Phys. A* 79 (2004) 1323–1326.
- [27] N.M. Bulgakova, A.V. Bulgakov, *Appl. Phys. A* 73 (2001) 199–208.
- [28] M. Stafe, A. Marcu, N. Puscas, *Pulsed Laser Ablation of Solids: Basics, Theory and Applications*, Springer, 2013.
- [29] G.V. Samsonov, *The Oxide Handbook*, IFI/Plenum, 1982.
- [30] A. Berthelot, F. Gourbilleau, C. Dufour, B. Domengès, E. Paumier, *Nucl. Instrum. Methods Phys. Res. B* 166–167 (2000) 927–932.